J Mater Sci (2009) 44:6372–6383
DOI 10.1007/s10853-009-3878-9

Effect of nitrogen and nickel on the microstructure and mechanical properties of plasma welded UNS S32760 super-duplex stainless steels

K. Migiakis · G. D. Papadimitriou

Received: 3 March 2009 / Accepted: 9 September 2009 / Published online: 23 September 2009

Abstract Super-duplex stainless steels present excellent combination of mechanical and corrosion resistance, due to their strict composition control and ferrite–austenite phase balance. This balance may, however, be disturbed during welding in both the fusion and HAZ due to the rapid cooling rates and may lead to loss of the good corrosion and mechanical properties of the weldments. The present investigation is studying the effect of nitrogen addition in the plasma operation gases and of the increase of nickel in the filler metal, on the microstructure and on the mechanical properties of super-duplex stainless steels welded by the plasma transferred arc (PTA) technique. Results have shown that nitrogen addition in the plasma operation gas affects the mechanical properties of the weldments. It is shown that nitrogen addition in the plasma and protective gas and higher nickel content in the filler metal have both a positive effect on the elongation of the welded specimens and after optimization of the welding parameters very good results may be obtained in terms of tensile strength.

Introduction

Duplex stainless steels are alloys consisting of a two phase microstructure with a balance between ferrite and austenite. They combine very good corrosion properties, high yield strength and good toughness in a wide temperature interval ranging from −50 to 250 °C. The so-called super-duplex stainless steel grades contain increased amounts of Cr, Ni, Mo and N and typically have pitting resistance equivalent number (PREN) greater than 40. Because of their higher alloy content, super-duplex stainless steels exhibit higher strength than the standard duplex alloys [1, 2]. Duplex stainless steels exhibit good weldability but there remain some problems in welding due to the increase of ferrite/austenite ratio in the fusion zone (FZ) and in the heat-affected zone (HAZ), which can lead to a decrease of pitting corrosion resistance of these alloys. The ferritization takes place as a consequence of high peak temperature and of the fast cooling rates of the thermal cycles [3–6]. It is, therefore, necessary to assure the continuity of the duplex microstructure across the welds, and this is in general achieved by controlling the cooling rate by using increased heat inputs. Nevertheless, high heat inputs promote the precipitation of harmful intermetallic phases, such as σ-phase, in the fusion zone of stainless steels and carbides, nitrides or other phases in the heat-affected zone of steels in general [7, 8]. This phenomenon is intense in super-duplex stainless steels which are highly alloyed with Cr, Mo, N and in some cases with Cu and W, too [9–12]. In order to obtain the desired phase balance, the addition of γ stabilizers, such as Ni in the filler metal and N in the shielding gas [13–15] are sometimes used. The addition of nitrogen through the shielding gas and its effect on the corrosion and mechanical properties of duplex stainless steel welds have been investigated in the case of TIG and MIG techniques [16–22]. The present work focuses on the addition of nitrogen in the plasma operation gas during plasma transferred arc welding (PTA). Plasma welding has significant advantages over conventional TIG in terms of productivity, penetration depth, thermal distortion and concentrated energy [23–25]. In the present work, the

K. Migiakis (✉) · G. D. Papadimitriou
Laboratory of Physical Metallurgy, National Technical University of Athens, 9 Iroon Polytechneiou Str., 15780 Zografou, Greece
e-mail: kmigiakis@metal.ntua.gr

G. D. Papadimitriou
e-mail: gpapadimitriou@metal.ntua.gr

effect of nitrogen addition during plasma welding with two different filler metals (of low and high nickel content) on the microstructure and on the mechanical properties of super-duplex stainless steels is investigated.

Experimental procedure

The material used for this research is a 6 mm thick plate of UNS 32760 super-duplex stainless steel (Zeron 100), provided by Weir Materials and Foundries. Two different types of filler metal were used. The first one (HNi) is a high Ni content filler metal and the other (BM) has exactly the same composition with the base metal. The chemical composition of the base metal and of the filler metals (wt%) is given in Table 1. Specimens were prepared for one sided butt welding joints, as shown in Fig. 1. Welds were produced using a PW-200 Sabre arc plasma console, a plasma torch (PWA-3A) and a KEMPI 2000 power source. All joints were made using backing equipment attached to the root side for protection of root joint. Four different types of gas mixtures were used as plasma and shielding gas. The mixtures used were pure Argon, 98%Ar–2%N, 95%Ar–5%N and 90%Ar–10%N. As backing gas the same mixture with the plasma operating gas was used, with a flow rate of 10 L/min. Welding conditions are given in Table 2. According to the welding designation, three passes were required to fill the gap. The interpass temperature was measured to be less than 150 °C using a contact thermocouple. The heat input was adjusted to 1 kJ/mm for the root pass, 0.8 kJ/mm for the second "cold" pass and 1 kJ/mm for the third pass, according to the guidelines for multipass welding of Zeron 100 DSS [26, 27].

From the welded coupons three groups of specimens were prepared, one for metallographic examination, the second for hardness measurement and the third for tensile testing. The samples were prepared by polishing and electrolytic etching with 20% KOH solution in water at a 3 V etching potential. Metallographic observation was carried out via light optical microscopy and scanning electron microscopy (SEM) with EDS microanalysis. The nitrogen content of the welds was measured using mass spectrography. The phase ratio between ferrite and austenite was measured by manual point counting according to the ASTM standard E 562-95 [28] and using an image analysis software. X-ray diffraction (XRD) analysis was used for characterization of the phases and for confirmation of the volume fractions of austenite and ferrite, as determined by quantitative metallography. XRD patterns were obtained using Cu-Kα radiation and the integrated intensity of the peaks corresponding to the (111), (200), (220) planes of austenite and of the peaks corresponding to the (110), (200), (211) planes of ferrite was measured. The austenite to ferrite ratio was then calculated according to ASTM E 975-95 standard [29]. The *R*-values corresponding to the composition of UNS S32760 steel for Cu-Ka radiation were calculated using data from International tables of X-ray crystallography [30] and shown in Table 3.

The Vickers hardness profile was measured on a cross section of the welds perpendicular to the welding direction, using a Shimatzu HMV–2000 equipment under a load of

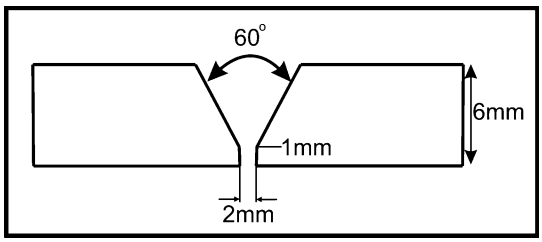

Fig. 1 Welding coupon

Table 2 Plasma welding parameters

Plasma welding conditions	
Welding current (A)	80
Welding speed V (mm/s)	2
Heat input (kJ/mm)	1
Plasma gas flow (L/min)	0.3
Shielding gas flow (L/min)	7
Arc length (mm)	2
Gas mixture(Shielding gas and plasma gas)	Pure Ar
	98%Ar–2%N
	95%Ar–5%N
	90%Ar–10%N
Tip diameter (mm)	2.06
Electrode diameter [W–2%Ce_2O] (mm)	2.56
Filler metal diameter (mm)	1.5

Table 1 Composition of the base metal and of the filler metals

Composition (%wt)	Parent material	Filler (HNi)	Filler (BMF)
C	0.02	0.015	Base metal
Si	0.37	0.31	
P	0.001	0.006	
S	0.002	0.02	
Mn	0.66	0.7	
Ni	6.9	9.23	
Cr	25.2	25.15	
Mo	3.7	3.16	
Cu	0.62	0.58	
W	0.63	0.62	
N	0.24	0.22	
Fe	Bal.	Bal.	

Table 3 *R* values of specific peaks for determining austenite/ferrite phase ratio according to ASTM E975-95

Peak	$(111)_\gamma$	$(200)_\gamma$	$(220)_\gamma$	$(110)_\delta$	$(200)_\delta$	$(211)_\delta$
R value	85.003	88.045	18.558	125.659	37.506	61.204

500 g applied for 15 s. Tensile specimens were prepared according to ASTM E8M [31] standard and the tensile tests were carried out at room temperature using an Instron 4482 machine. The fracture surfaces of the specimens after tensile testing were examined via scanning electron microscopy.

Results and discussion

Metallographic examination

The microstructure of UNS 32760 in the as received state consists practically of equal amounts of austenite and ferrite, Fig. 2. No other phases are observed. After welding, this balance is disturbed in the fusion zone. Table 4 shows the corresponding volume fractions of austenite and ferrite in the parent metal and in specimens welded with both BM and HNi filler metals and with the different gas mixtures: Ar, 98%Ar–2%N, 95%Ar–5%N and 90%Ar–10%N. In the same table the nitrogen content of the parent material and of the fusion zone of the weldings is shown.

From Table 4 it is evident that a significant amount of nitrogen passes from gas mixtures containing nitrogen into the fusion zone and that the nitrogen content of the weld

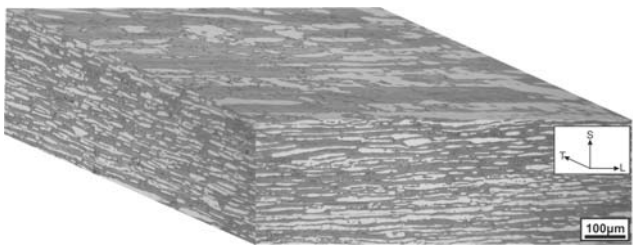

Fig. 2 Three-dimensional representation of the microstructure of UNS 32760 super-duplex stainless steel

metal increases with nitrogen content in the plasma operating gas. This increase is in principle expected, since under equilibrium conditions the solubility of nitrogen in a molten metal is proportional to the square root of its partial pressure in the gas phase [32]. However, several authors have pointed out that nitrogen absorption by a weld metal is enhanced above the equilibrium solubility of nitrogen predicted by Sieverts law [33–35]. This is due to the existence of monatomic nitrogen in the plasma arc. As a matter of fact, the high temperature developed in the plasma constricted arc favours the dissociation of molecular to monatomic nitrogen. Considering the free energy change $\Delta G_T^0 = 86596–15659\ T$ (cal/mol) of the reaction $N_2 \rightarrow 2N$ [36], which is based on thermodynamic data from the compilation by Elliott and Gleiser [37], it comes out that the dissociation of diatomic to monatomic nitrogen is favoured above 5530 °K. Temperatures in the range of 7000–10000 °K and even higher have been determined in the plasma/weld pool interface in the GMA welding arc [38]. According to Hertzman et al. [16], for pure nitrogen dissociation starts above roughly 4000 °K and is fairly complete at temperatures above 10000 °K, implying that in a flame the nitrogen is hardly dissociated at all, whereas at temperatures encountered in the plasma of a gas-shielded arc column the nitrogen is fully dissociated. Wei Dong et al. [39] were able to demonstrate experimentally the presence of monatomic nitrogen coming from dissociation of molecular nitrogen over the bath of laser CO_2 welding by using monochromatic images of a specific spectrum line emitted by monatomic nitrogen.

According to Debroy et al. [36], the equilibrium concentration of nitrogen in solution in iron melt is considerably higher in the monatomic gas environment than in the corresponding diatomic gas environment. As it comes out from the free energy change $\Delta G_T^0 = -85736 + 21405\ T$ (cal/mol) of the reaction $N(g) \rightarrow \underline{N}$ [36], based on thermodynamic data from the compilation by Elliott and Gleiser (1960), the dissolution of monatomic nitrogen in iron is possible at temperatures below 4005 °K and increases rapidly as the temperature falls below 2000 °K. Although above the bath the plasma gas reaches temperatures of several thousands °K, the temperature of the melt is much lower. In the case of iron alloys it remains below 2000 °K,

Table 4 Austenite fraction (vol%) and nitrogen content (wt%) in the parent metal and in the fusion zone of weldings for different combinations of filler metal and PTA operating gas mixtures

	Parent metal	Ar fusion zone		98%Ar–2%N fusion zone		95%Ar–5%N fusion zone		90%Ar–10%N fusion zone	
		BMF	HNi	BMF	HNi	BMF	HNi	BMF	HNi
γ-fraction (vol%) quantitative metallography	52.2	37.8	45.1	50.2	75.3	72.7	83.0	79.2	88.9
Nitrogen content (%wt)	0.243	0.217	0.212	0.297	0.314	0.412	0.418	0.482	0.478

allowing the dissolution of nitrogen in the bath according to the reaction N(g) → N. As a matter of fact, it was shown [34, 40] that during tungsten arc melting of iron alloys containing chromium and nickel under argon–nitrogen gas atmospheres, the temperatures measured always remained below 1950 °K.

From Table 4 it becomes evident that the nitrogen content of the weld metal depends mainly on the composition of the operating gas, irrespective of the type of filler metal (BM or HNi) used in the present investigation. This is in agreement with the results of Kuwana et al. [34], who observed that during GTAW welding of Fe–Ni alloys, the nickel content of the base metal does not affect significantly the nitrogen content of the weld. As a matter of fact, only a slight decrease of nitrogen in the weld metal is observed with increasing nickel content.

In the present investigation, when welding was performed with argon, a reduction of the nitrogen content in the fusion zone with respect to the parent material was observed (Table 4). Nitrogen loss should be attributed to the difference in partial pressure between the nitrogen dissolved in the weld pool and in the operating gas. The extent of nitrogen loss is dependent on the welding parameters and on the nitrogen content of the steel [41]. In this case, when BM filler type is used, the balance between the two phases is disturbed, resulting in a dominant ferritic microstructure with 37.8% austenite, Fig. 3a. This is due not only to loss of nitrogen which is a γ-stabilizer, but also to the high cooling rates associated with welding and to the small amount of γ-stabilizers in the composition of the filler metal.

The microstructure obtained for the specimens welded with BM-filler metal and with various additions of nitrogen in the operation gas is shown in Fig. 3b–d. It is clearly seen that the increase of nitrogen content in the operation gas leads to a higher austenite content in the microstructure. This is also shown in Table 4 and is schematically represented in Fig. 4. Using 2%N in the plasma operation gas, the balance between austenite and ferrite (50/50 vol% fraction) seems to be reached. The amount of austenite attains 72.7% when the gas mixture is 95%Ar–5%N and 79.2% in the case of 90%Ar–10%N. The results obtained here are comparable to those obtained with MIG [17, 19] and TIG welding [21], but the strong dissociation of molecular nitrogen at the temperatures of plasma arc seems more effective in introducing nitrogen in the weld metal.

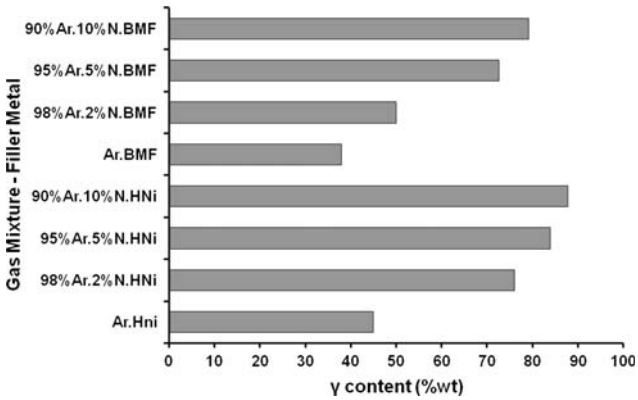

Fig. 4 Effect of nitrogen and nickel addition on the austenite content in the fusion zone by using both BMF- and HNi-filler metals and different gas mixtures as operating gas

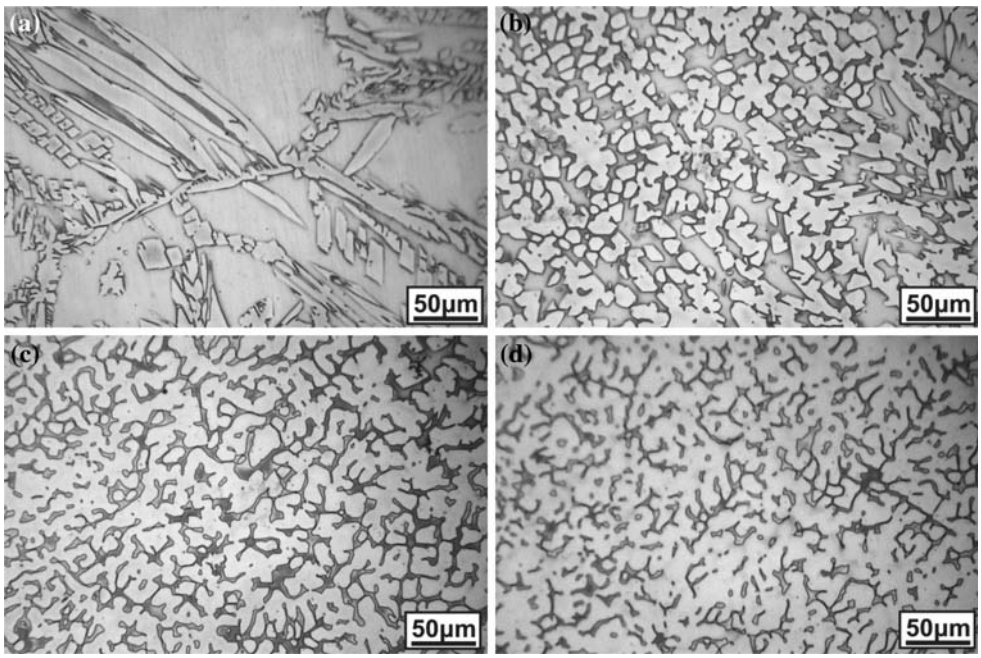

Fig. 3 Microstructure of fusion zone with BMF as filler metal and with various compositions of the operation (plasma and protective) gas **a** Ar **b** 98%Ar–2%N **c** 95%Ar–5%N and **d** 90%Ar–10%N

As a result, only 2% nitrogen in the gas mixture is sufficient to preserve the γ/δ phase balance.

The increase of the austenite content in the fusion zone is more pronounced when the rich in nickel filler metal (HNi) is used in association with the same as above gas mixtures. Figure 5a–d shows the corresponding microstructures of the fusion zones obtained, whereas quantitative results are again represented in Fig. 4.

In this case, welding with pure Argon leads to 45.1% austenite in the fusion zone. Using 98%Ar–2%N in the operation gas leads to 75.3% austenite, using 95%Ar–5%N leads to 83% austenite and using 90%Ar–10%N leads to as high as 88.9 austenite in the fusion zone.

XRD analysis of the welded specimens was used to confirm the results obtained with quantitative metallography. Figure 6 shows, as an example, XRD spectra of base metal and of specimens welded with BMF as filler metal and with different gas mixtures as operating gas. This analysis showed the presence of austenite in increasing amounts as the gas mixture becomes richer in nitrogen. In this respect, the ferrite fraction of the specimens was also estimated using the WRC-1992 ferrite number (FN) diagram and the Shaeffler-Delong diagram [42, 43]. The results obtained by using all the above mentioned methods are shown in the comparative Table 5.

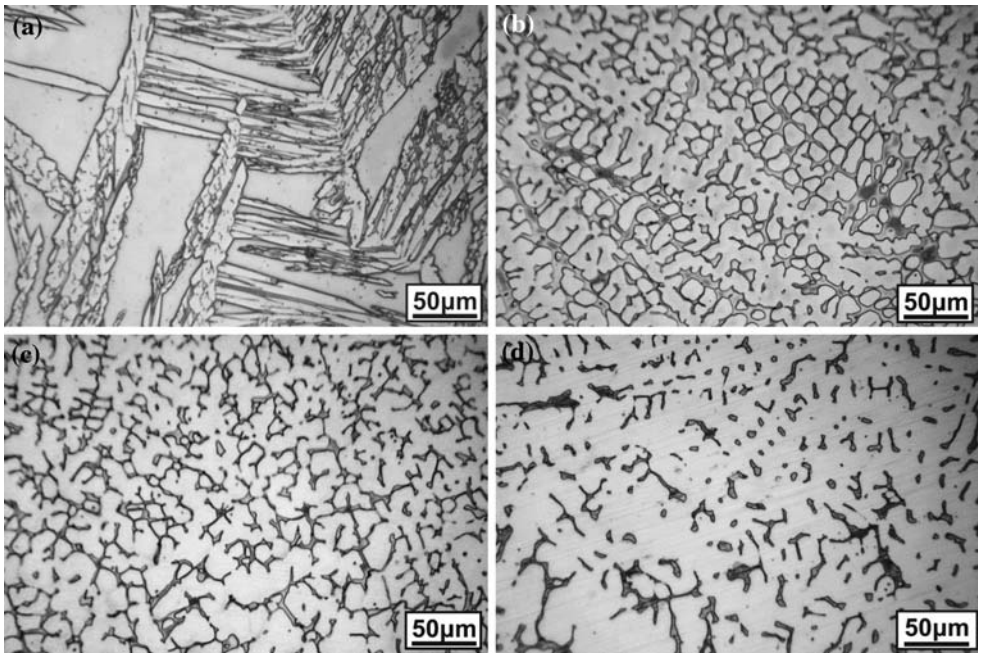

Fig. 5 Microstructure of fusion zone with HNi as filler metal and with various compositions of the operation (plasma and protective) gas **a** Ar **b** 98%Ar–2%N **c** 95%Ar–5%N and **d** 90%Ar–10%N

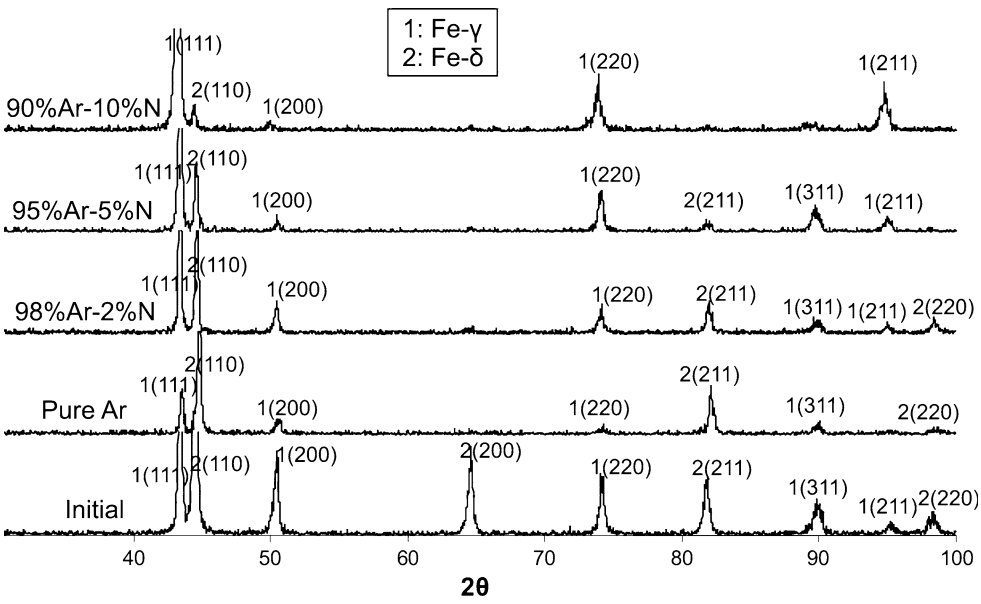

Fig. 6 XRD spectra of base metal and welded specimens with BMF as filler metal and with different gas mixtures as operating gas

Table 5 Ferrite fractions, as determined by quantitative metallography and by XRD analysis

δ%	Ar		98%Ar–2%N		95%Ar–5%N		90%Ar–10%N	
	BM	HNi	BM	HNi	BM	HNi	BM	HNi
Determined by quantitative metallography [28]	62.2%	54.9%	49.8%	24.7%	27.3%	17%	20.8%	11.1%
Determined by XRD [29]	63.9%	53.3%	48.3%	23.9%	26.3%	17.4%	16.6%	10.5%
WRC-1992 Ferrite number (FN) [42]	78	56	64	34	38	22	27	16
WRC-1992 δ% [44]	58%	46%	49%	32%	34%	22%	27%	17%
Shaeffler-Delong δ% [43]	38%	31%	29%	26%	25%	15%	17%	10.5%

Corresponding values predicted with WRC-1992 [42] and Schaeffler-Delong diagrams [43]

From this table it comes out that ferrite contents obtained by using either quantitative metallography or X-ray diffraction are comparable. The ferrite number (FN) calculated according to [42] gives too high figures for ferrite content. If however a correction of the FN is applied according to Palani et al. [44], ferrite contents closer to the results of quantitative metallography are obtained. Finally, the previsions based on the Schaeffler-Delong diagram are in general inconsistent with the results of quantitative metallography, except for ferrite contents of the order of 25% and lower. As a matter of fact, the Shaeffler-Delong diagram was developed as a prediction tool for conventional austenitic and other stainless steels, but it is not convenient to predict duplex microstructures. On the other hand, the WRC-1992 diagram provides better prediction for duplex microstructures [3].

From the above results it is concluded that nitrogen addition in the plasma operating gas during welding of UNS 32760 super-duplex stainless steel promotes the $\delta \rightarrow \gamma$ transformation, resulting in increase of the austenite content. The increase of austenite fraction in the fusion zone is due not only to the action of nickel and nitrogen as gamma-stabilizing elements, but also to the ability of nitrogen in shifting the ferrite–austenite solvus in a way that the $\delta \rightarrow \gamma$ transformation starts at higher temperatures [45]. Furthermore, nitrogen containing gases have higher ionization potential than pure argon and result to an increase of heat input, which contributes in obtaining lower cooling rates [46]. Thus the δ to γ transformation begins earlier and despite the high cooling rates prevailing in welding, more time is available for the transformation to approach the equilibrium values.

From micrographs of Figs. 3 and 5 it is observed that the absorption of nitrogen in the weld metal leads to transition from the characteristic acicular austenite microstructure obtained when welding with pure argon to mostly globular morphologies occurring when using nitrogen containing mixtures. This is in agreement with previous investigations [21, 47].

In the case of specimens welded with pure argon the presence of secondary austenite γ_2 is observed within the ferrite grains in the interpass regions of the fusion zone, as shown in Fig. 7. It is, however, advantageous that secondary austenite is not present in the interpass regions when nitrogen is added in the operating gas during plasma welding.

In the heat-affected zone (HAZ) the 50:50 phase balance between austenite and ferrite is in general disturbed for all weldments, with ferrite occupying the largest volume fraction. The microstructure consists of grain boundary allotriomorphs and Widmanstatten needles of austenite inside the ferrite grains. The presence of secondary austenite is also observed. However, for the specimens welded with mixtures containing nitrogen, a slight improvement of the microstructure is observed even in the case of the heat-affected zone. As a matter of fact, in this case, the amount

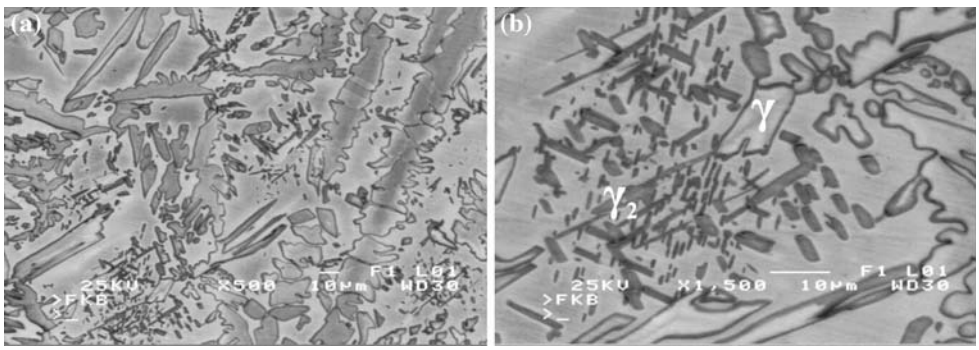

Fig. 7 SEM images. Presence of secondary austenite in the interpass region of the fusion zone with BMF as filler metal and Argon as operation gas

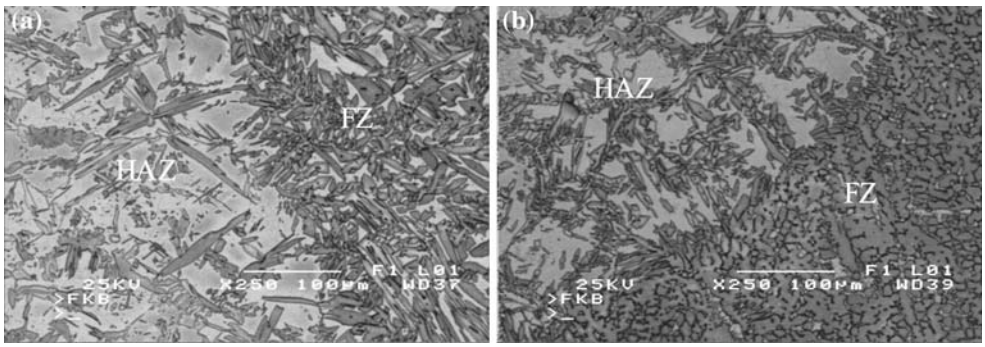

Fig. 8 SEM images of HAZ-fusion zone with HNi as filler metal and **a** Ar as operating gas **b** 98%Ar–2%N mixture as operating gas

of secondary austenite seems to be lower, compared to the amount of secondary austenite of the specimens welded with pure Ar, as shown in Fig. 8. This demonstrates that some nitrogen diffuses into the heat-affected zone during welding.

A common phenomenon when welding super-duplex stainless steels is the presence of harmful precipitates in the fusion zone [2]. SEM observation of the specimens revealed the fusion zone and the HAZ free of σ-phase particles for all welded specimens. However, detailed SEM examination allowed detecting the presence of intragranular nitrides within ferrite grains in the HAZ of specimens welded with 90%Ar–10%N gas mixtures, Fig. 9a, b. The precipitation of these nitrides is presumably due to the relatively high nitrogen content absorbed by the HAZ of the weldment, when a high nitrogen gas mixture is used. Ramirez et al. [48] have observed that during heat treatments of DSS in the temperature range of 1100–1200 °C, intragranular Cr_2N nitrides precipitated within the ferrite grains and intergranular Cr_2N nitrides developed in ferrite/primary austenite interfaces. The latter facilitated the precipitation of secondary austenite ($\gamma 2$) in the ferrite/Cr_2N interfaces. In our case, nitrides were observed mainly within the ferrite grains of the HAZ and seem associated with local formation of secondary austenite around them, as it is observed in the BEI of Fig. 9b.

A very fine and dense dispersion of submicron size nitrides was also detected in the HAZ of specimens welded with pure argon, as shown in Fig. 9c, d. However, detailed SEM examination of weldments done with 2 and 5% nitrogen showed that both the fusion and heat-affected zone were free of nitrides. This corroborates the hypothesis that during plasma welding with nitrogen containing mixtures, some nitrogen diffuses also into the HAZ. Matsunaga et al. [49] observed that the addition of nitrogen during TIG welding of duplex stainless steels leads to a decrease of

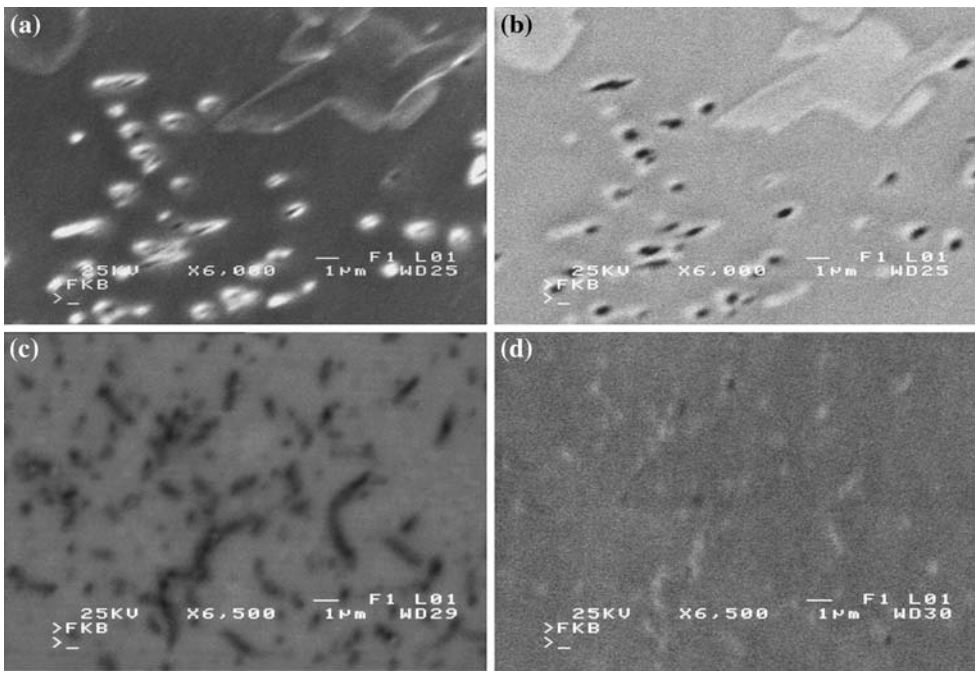

Fig. 9 SEM micrographs showing chromium nitrides within ferrite in the HAZ of weldments **a** and **b** Secondary electron and corresponding backscattered electron image of specimen welded with BM-filler metal and 90%Ar–10% N operating gas. **c** and **d** Secondary electron image (reverse polarity) and corresponding backscattered electron image of specimen welded with pure argon

chromium nitrides in the weldment. Since with increasing nitrogen content the transformation $\delta \rightarrow \gamma$ occurs at higher temperatures, the diffusion of nitrogen is easier and longer, so that more time is available for the migration of nitrogen from ferrite to austenite. Thus a lower content of nitrogen in ferrite will result in a decrease of nitride precipitation within it.

Mechanical properties

Hardness

Figure 10 shows hardness profiles of specimens welded with both BMF- and HNi-filler metals. The Vickers hardness of the base metal is about 274 HV. In the heat-affected zone of all specimens the hardness decreases due to the growth of ferrite grains, which lead to lower values with an average of 266 HV. In the fusion zone an increase of the hardness of all specimens is observed and according to Gunn [3] it should be attributed to the strain induced by the heating and cooling cycle. Furthermore, the absorption of nitrogen acts by increasing the austenite to ferrite ratio and by strengthening the austenite. Hence the hardness of the fusion zone increases with nitrogen content, since austenite dissolves most of nitrogen present in the weld metal. More specifically the Vickers hardness of the specimens welded with BM as filler metal and pure argon is about 284 HV and it reaches 291 HV for the specimens welded with the same filler metal and 90%Ar–10%N mixture. It is also observed that a higher nickel content in the filler metal leads to a slightly lower value of hardness.

Tensile test results

The tensile properties of the specimens were measured in terms of yield strength, tensile strength and ductility. Eight coupons were tested for each parameter. In Table 6 the resulting mean values and corresponding standard deviations are given. All reference samples of parent metal failed in the middle of the gauge length. In the case of 98%Ar–2%N operating gas, failure always occurred in the parent material. The poorest behaviour, in terms of failure

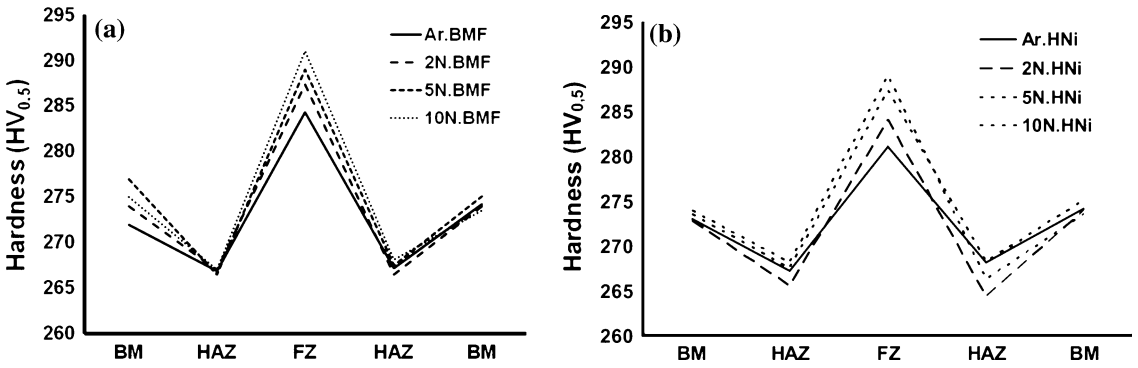

Fig. 10 Vickers hardness profiles on cross sections of specimens welded with various nitrogen contents in the operating gas and **a** BMF as filler metal and **b** HNi as filler metal

Table 6 Tensile properties for parent metal and welded specimens

Specimen	*N* %	% vol γ and microstructure	$Rp_{0.2}$ (MPa)*	Rm (MPa)*	e %*	Failure area (No of specimens on eight tests)	
						Parent metal	Weld metal
Parent material	0.243	52.2 layered	642 ± 8.2	850 ± 12.7	33.3 ± 1.23	8	–
Ar.BMF	0.217	37.8 widmanst	627 ± 14.8	860 ± 28.2	17.4 ± 4.32	2	6
98%Ar–2%N.BMF	0.297	50.2 globular	667 ± 10.2	878 ± 22.1	27.1 ± 1.62	8	0
95%Ar–5%N.BMF	0.412	72.7 globular	657 ± 9.3	865 ± 23.4	26.5 ± 2.96	6	2
90%Ar–10%N.BMF	0.482	79.2 globular	680 ± 11.4	879 ± 25.5	23.3 ± 4.55	3	5
Ar.HNi	0.212	45.1 widmanst	619 ± 15.5	837 ± 23.1	19.2 ± 5.13	2	6
98%Ar–2%N.HNi	0.314	75.3 globular	661 ± 11.3	874 ± 19.5	27.75 ± 1.54	8	0
95%Ar–5%N.HNi	0.418	83.0 globular	658 ± 15.9	855 ± 17.6	28.2 ± 2.27	7	1
90%Ar–10%N.HNi	0.478	88.9 globular	676 ± 16.2	880 ± 27.8	25.05 ± 4.74	4	4

* Each result represents an average over eight mechanical tests

position, presented the specimens welded with Ar, which failed mostly in the weld area, irrespective of the filler metal used. In this case only 25% of the specimens presented failure in the parent material. The specimens welded with 90%Ar–10%N, did not present good behaviour in terms of failure position, irrespective of the filler metal used. Only 37.5% of the specimens welded with a BM-filler metal and 50% of the specimens welded with a HNi-filler metal have failed in the parent material. It must be, however, noted that in all weldments performed with either argon or with a nitrogen containing mixture, failure occurred at a stress level higher than the proof stress of the parent material. Regarding the 0.2% proof stress, all welded specimens have resulted in values above 600 MPa.

When pure argon was used in the operating gas, the lowest values of elongation were observed. The elongation of the welded specimens increased with increasing nitrogen content in the operating gas, except in the case of 90%Ar–10%N where the elongation presented somewhat lower values, irrespective of the filler metal used. Comparing the specimens welded with BMF- and HNi-filler metal there was no significant difference in the tensile strength obtained, except in the case of welding with pure argon, where a decrease was obtained when a filler metal with higher nickel content was used. An increase in elongation was also observed, when higher nickel filler metal was used in the weldment. Typical tensile test diagrams are given in Fig. 11a, b. Figure 11a concerns cases where fracture occurred in the parent metal of the weldments, whereas Fig. 11b concerns cases where fracture occurred within the weld area. In the latter case elongation was found significantly diminished.

In trying to interpret the mechanical properties measured, it should be considered that the nitrogen content may affect both positively and negatively the mechanical properties of the weldments. As a matter of fact, nitrogen affects the austenite to ferrite ratio, it modifies the microstructure and may eventually cause the formation of nitrides. Nitrogen exerts also a direct strengthening effect on both the α and γ phases, but mainly on austenite [50]. In the case of the BM-filler metal, weldments done with 2 or 5% nitrogen show clearly improved properties with respect to weldments done with argon. As a matter of fact, both yield strength and elongation are greater in weldments done with a nitrogen containing mixture than in the corresponding ones obtained with argon. The tensile strength is also slightly improved in weldments done with nitrogen in the gas mixture.

The increased yield strength should be attributed to the higher austenite to ferrite ratio (50.2 and 72.7 vol%, respectively, for 2 and 5% nitrogen in the gas, compared to 37.8 vol% in the case of the argon operation gas) and to the increased hardness of austenite enriched with nitrogen. Since nitrogen is a γ-stabilizer, most nitrogen atoms tend to dissolve in the γ-phase. Therefore the effect of interstitial solution strengthening by nitrogen is more pronounced in γ-phase than in α-phase.

Different mechanisms have been proposed in order to explain the hardening effect of nitrogen on austenite. Rawers et al. [51] reported that the yield strength of

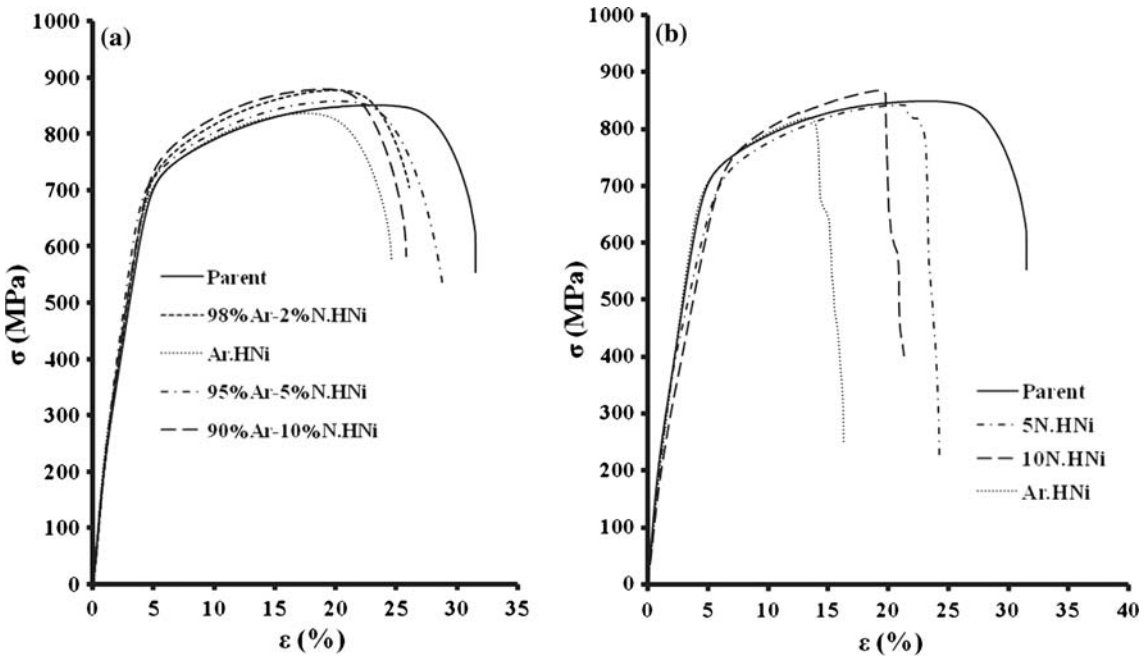

Fig. 11 Tensile diagrams of parent metal and specimens welded with HNi filler. Failure area: **a** parent metal **b** welded metal

austenitic stainless steel increases with nitrogen content as a result of two strengthening mechanisms: (a) matrix strengthening due to interaction between interstitial nitrogen and dislocation motion, which is proportional to $[N]^{1/2}$, and (b) dislocation–nitrogen drag interaction, resulting from the nitrogen being carried along the dislocation as it moves in the lattice, which is proportional to [N].

On the other hand, in order to account for the increased ductility, one should consider the modification of the stacking fault energy of austenite with the nitrogen content. According to Pickering [52], the stacking fault energy of a stainless steel decreases with nitrogen content. As a consequence, with increasing nitrogen content the separation between two partial dislocations will be broader, causing the dislocations to be confined to their slip plane and to form pile-ups. This in turn, gives rise to higher work hardening rate, tensile strength and uniform elongation.

Furthermore, in explaining the higher ductility of the weldments done with a nitrogen containing gas mixture, the morphology of the phases present should not be disregarded. Austenite presents a Widmanstatten morphology in weldments done with argon, but it has a globular morphology in weldments done with a nitrogen containing mixture, as it was reported in the section of microstructure. Almost all tensile specimens welded with 2 and 5% nitrogen, irrespective of the filler metal used, have broken in the base metal, outside the welding zone. This was due to the fact that besides a satisfactory yield and tensile strength, the corresponding weldments possessed also an elevated ductility (27.1 and 26.5%, respectively, in BMF weldments done with 2 and 5% nitrogen in the operating gas). On the contrary, the ductility of the weldments done with argon was much lower (17.4 and 19.2%, respectively, for BMF- and HNi-filler metal) and this caused breaking of the majority of specimens in the weld metal. The low ductility of these specimens should be attributed to several reasons: (a) to the Widmanstatten morphology of austenite (Fig. 3a and 5a), (b) to the presence of secondary austenite in the interpass regions (Fig. 7a, b) and (c) to the precipitation of nitrides in the heat-affected zone (Fig. 9a–d). These factors should explain the fracture of most specimens welded with argon within the welding zone.

The specimens welded with 10% argon showed the highest yield (and tensile) strength, but a reduced ductility (23.3%) with respect to specimens welded with 2 and 5% nitrogen. About half of them have broken in the welding zone, since this area possessed a reduced ductility with comparison to the parent metal. This should be attributed to the extremely high nitrogen content of the welding zone which caused an excessive strengthening effect and presumably hindered the motion of dislocations. Furthermore, the presence of Cr_2N precipitates in the heat-affected zone should also be considered as responsible for the low ductility observed in these specimens.

Considering the weldments done with a HNi-filler metal, the results of mechanical tests are qualitatively very similar to those described above, although in general their strength is somewhat lower and their ductility slightly better than in corresponding weldments done with a BM-filler metal. This should be attributed mainly to their higher austenite content compared to weldments done with a BM-filler metal. Therefore, since the nitrogen content is almost the same in both cases (see Table 4), this means that austenite has a slightly lower nitrogen content in HNi weldments than in corresponding BM weldments. As a result, the presence of a lower nitrogen content in austenite presumably causes a slightly lower yield and tensile strength, but a somewhat higher ductility in weldments done with HNi-filler metal.

Fracture surfaces of the tensile specimens were examined via SEM. The fracture area of weldments that failed in the parent material exhibited exclusively ductile type fracture with equiaxed dimple type morphology, Fig. 12a. Specimens welded with pure Ar in the operating gas and for both types of filler metal presented all a mixed type of fracture. In this case the major part of the fracture area exhibited dimple type morphology, but there were some areas with cleavage type fracture, as shown in Fig. 12b, e. Specimens welded with 95%Ar–5%N presented ductile fracture with dimple type morphology and narrower dimples with regard to the parent material, Fig. 12d. When 90%Ar–10%N was used in the operating gas, the major part of the fracture area consisted of dimple type ductile morphology, but there were also areas with mixed type of fracture, Fig. 12c, f. These results are consistent with the mechanical properties measured in the same specimens and in particular with ductility.

Conclusions

Nitrogen addition in the plasma operating gas during plasma welding of UNS 32760 super-duplex stainless steel promotes the increase of austenite content in the microstructure of the fusion zone and at the same time leads to the formation of globular morphology of austenite. Secondary austenite forms in the multipass regions of the fusion zone when pure Ar is used and is absent when nitrogen is added in the plasma operating gas.

A balanced microstructure with 49.8% austenite and 50.2% ferrite is obtained using an operating gas mixture of 98%Ar–2%N with a welding filler metal having a composition similar to that of the parent metal.

Nitrogen addition in the plasma gas increases slightly the hardness of the fusion zone with regard to the hardness

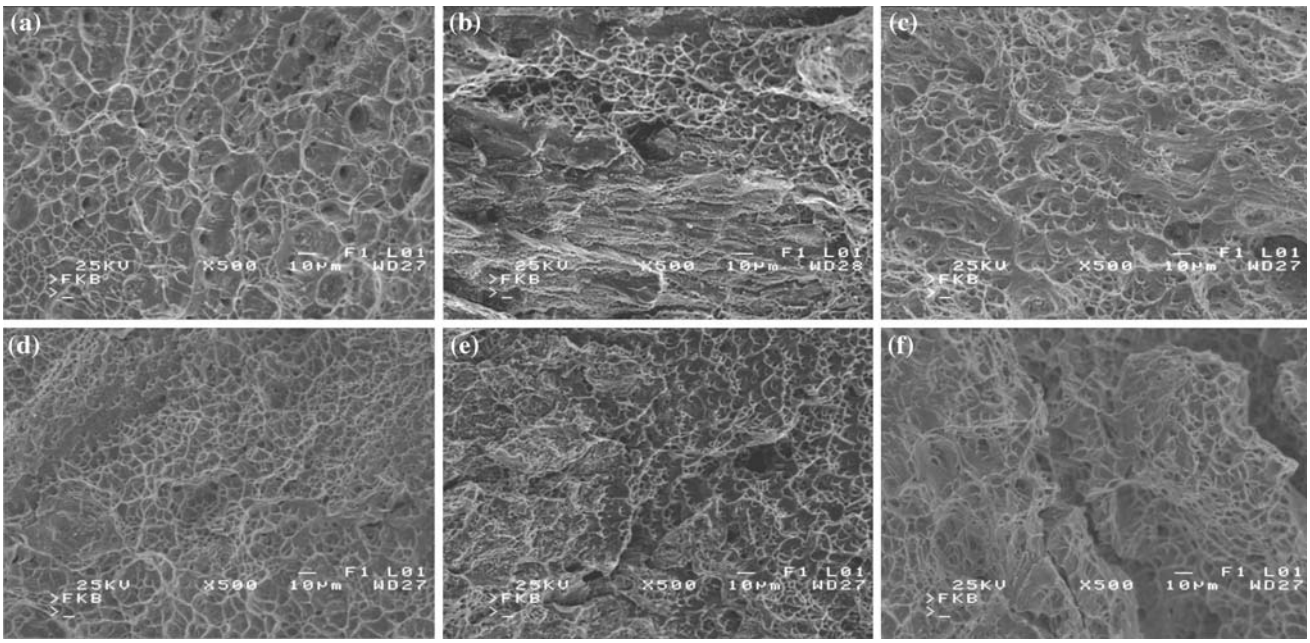

Fig. 12 Fracture surfaces of **a** Parent material **b** BMF, Ar **c** BMF, 90%Ar–10%N, **d** HNi, 95%Ar–5%N **e** HNi, Ar **f** HNi, 90%Ar–10%N

of the base metal. In the contrary, when a higher nickel content is used in the filler metal the hardness slightly decreases. In the heat-affected zone the hardness is lower than the hardness of the base metal due to the growth of ferrite grains.

The best results in tensile testing were obtained from specimens welded with 98%Ar–2%N. These specimens did not present failure in the welded area.

The poorest behaviour during tensile testing was obtained from specimens welded with pure Ar, due to the Widmanstätten morphology of austenite, to the presence of secondary austenite in the interpass regions of the fusion zone and to the presence of nitrides in the HAZ. Relatively low ductility was also exhibited by welds done with a mixture of Ar–10%N, due to the presence of nitrides in the HAZ. However in all cases final fracture occurred at a stress level higher than the proof stress of the parent material.

Nitrogen and nickel addition during plasma welding resulted in an increase of the ductility of the welded specimens.

Fracture surfaces of parent metal and of welded specimens with 98%Ar–2%N and with 95%Ar–5%N presented exclusively ductile fracture with dimple type morphology. Dimple type morphology with some areas of mixed ductile and brittle fracture was exhibited by specimens welded with 90%Ar–10%N. Finally, specimens welded with pure Ar presented mixed type of ductile and brittle fracture.

References

1. Charles J (1994) Proc. Duplex stainless steels ‘94 Glascow Scotland: paper KI
2. Nilsson JO (1992) Mater Sci Tech 8:685
3. Gunn RN (1997) Duplex stainless steels, microstructure properties and applications. Abington Publishing, Cambridge, England
4. Fourie JW, Robinson FPA (1990) J S Afr Inst Min Metall 90(3):59
5. Muthupandi V, Srinivasan PB, Seshadri SK, Sundaresan S (2003) Mater Sci Eng A358:9
6. Sathiya P, Aravindan S, Noorul Haq A (2009) J Mater Sci 44:114. doi:10.1007/s10853-008-3098-8
7. Wang HR, Wang W (2009) J Mater Sci 44(2):591. doi:10.1007/s10853-008-3069-0
8. Avazkonandeh-Gharavol M, Haddad-Sabzevar M, Haerian A (2009) J Mater Sci 44(1):186. doi:10.1007/s10853-008-3103-2
9. Lippold JC, Lin W, Brandi S, Varol I, Baeslack WA (1994) Proc. Duplex stainless steels ‘94 Glascow Scotland: paper 116
10. Gunn RN (1994) Proc. Duplex stainless steels ‘94 Glascow Scotland: paper 32
11. Huntala T, Nilsson J-O, Wilson A, Jonsson P (1994) Proc. Duplex stainless steels ‘94, Glascow Scotland: paper 43
12. Hertzman S, Nilsson M, Jargelius-Pettersson R (1994) Proc. Duplex stainless steels ‘94 Glascow Scotland: paper I
13. Bradshow R, Cottis A (1993) Weld Met Fabr 62(9):129
14. Wiktorowicz R, Crouch J (1993) Weld Met Fabr 62(9):379
15. Bekkers K, Hikes J, van Nassau L (1994) Proc. Duplex stainless steels ‘94 Glascow Scotland: paper 118
16. Bhatt R, Kamat H, Ghosal S, De P (1999) J Mater Eng Perf 8(5):591
17. Pak S, Karlsson L (1990) Scand J Met 19:9
18. Hertzman S, Jargelius-Pettersson R, Bom R, Kivineva E, Ericksson J (1996) ISIJ Int 36(7):968

19. Gomez de Salazar JM, Soria A, Barrena MI (2007) J Mater Sci 42:4892. doi:10.1007/s10853-006-0557-y
20. Muthupandi V, Bala Srinivasan P, Seshadri SK, Sundaresan S (2003) Corr Eng Sci Tech 38(4):303
21. Munoz I, Garcia J, Guinon JL, Herranz P (2005) Corrosion 61(7):693
22. Muthupandi V, Bala Srinivasan P, Seshadri SK, Sundaresan S (2004) Sci Tech Wel Join 9(1):47
23. O'Brien RL (1991) Weld handbook, vol 2, 8th edn. AWS, Miami, Fla
24. Zhang YM, Zhang SB (1999) Weld J 78(2):53
25. Taban E (2008) J Mater Sci 43:4309. doi:10.1007/s10853-008-2632-z
26. Zeron 100 welding guidelines, Weir Mater and Foundries (WMF), Mancester, UK, available at http://www.weirmaterials.co.uk
27. Baxter CFG, Stevenson AW, Warburton GR (1993) Proc. 3rd Int. Offshore and Polae Eng. Conf., Singapore, 6–11 June, p 408
28. ASTM E 562-95 (1995) Determining volume count by systematic manual point count
29. ASTM E 975-95 (2000) Standart practice for X-ray determination of retained austenite in steel with near random crystallographic orientation
30. Lonsdale K (1962) International tables for X-ray crystallography, vol III. Kynoch Press, Birmingham, England
31. ASTM E8M-08 (1997) Standard test methods for tension testing of metallic materials
32. Kou S (1987) Welding metallurgy. Wiley, New York, p 239
33. Palmer TA, Debroy T (2000) Metall Mater Trans B 31B:1371
34. Kuwana T, Kokawa H, Naitoh K-I (1990) Trans Jpn Weld Soc 21(2):157
35. Du Toit M, Pistorius PC (2003) Weld J 82(8):219s
36. Debroy T, David SA (1995) Rev Mod Phys 67(1):85
37. Elliott JF, Gleiser M (1960) Thermochemistry for steelmaking. Addison-Wesley Publishing Company, Reading, USA, p 74
38. Alfaro SCA, Mendoca D, Matos MS (2006) J Mater Proc Tech 179:219
39. Dong W, Kokawa H, Tsukamoto S, Sato YS, Ogawa M (2004) Metall Mater Trans B 35B:331
40. Kuwana T, Kokawa H, Muramatsu N (1989) Trans Jpn Weld Soc 20(1):10
41. Gunn RN, Anderson PCJ (1994) Proc. Duplex stainless steels '94, Glascow Scotland: paper 30
42. Kotecki DJ, Siewert TA (1992) Weld J 71(5):171s
43. De Long WT (1956) Weld J 35:521
44. Palani PK, Murugan N (2006) Mater Manuf Proc 26:431
45. Muthupandi V, Bala Srinivasan P, Shankar V, Seshadri SK, Sundaresan S (2005) Mater Lett 59:2305
46. Gavriljuk VG, Berns H (1999) High nitrogen steels, structure, properties manufacture and applications. Springer-Verlag, Berlin
47. Elmer JW, Allen SM, Eagar TW (1989) Metall Trans A 20(10): 2117
48. Ramirez AJ, Lippold JC, Brandi SD (2003) Metall Mater Trans A 34(A):1575
49. Matsunaga H, Sato YS, Kokawa H, Kuwana T (1998) Sc Tech Weld Join 3(5):225
50. Tseng CM, Liou HY, Tsai WT (2003) Mater Sci Eng A344:190
51. Rawers J, Gruijicic M (1996) Mater Sci Eng A207:188
52. Pickering FB (1985) Proc. stainless steels 84 Goteborg, 3–4 Sept 1984, The Institute of Metals, London, UK, p 12